34th Annual International Conference of the IEEE EMBS
San Diego, California USA, 28 August - 1 September, 2012

Nanodiamond Imaging: A New Molecular Imaging Approach*

Alex N. Hegyi, *Member, IEEE*, and Eli Yablonovitch, *Fellow, IEEE*

***Abstract*— A new molecular imaging approach is proposed that combines optical detection and magnetic field gradients to achieve high sensitivity and high spatial resolution. Called Nanodiamond Imaging, this new modality images the location of nanodiamonds within a living organism. Since nanodiamonds can be tagged with biologically active molecules and are nontoxic, Nanodiamond Imaging may become an important biomedical research tool with possible clinical application. A Nanodiamond Imaging system actually senses a particular type of defect in the nanodiamond called the nitrogen-vacancy center. A prototype system has been built that was tested by imaging an artificial target within a volume of chicken breast. The resolving power should be <100 µm with modest improvements, significantly finer than PET, SPECT, and in-vivo optical imaging. The sensitivity of the imaging system, taking into account foreseen improvements, should be better than a 10 nanomolar concentration of carbon atoms, referenced to a 1 mm^3 voxel volume and one second of measurement time (10 nM·mm^3·Hz$^{-1/2}$)—a similar sensitivity to the other molecular imaging techniques, but with a stable, non-radioactive tracer.**

I. Introduction

There exists an array of preclinical small-animal imaging modalities that address a range of imaging tasks [1], [2]. Structural or anatomical imaging techniques, such as magnetic resonance imaging (MRI), x-ray computed tomography (CT), and ultrasound (US), have sufficiently high resolution to provide anatomically relevant detail, but lack high sensitivity for imaging molecular processes. Conversely, techniques such as positron emission tomography (PET), single-photon emission computed tomography (SPECT), and photoluminescence or bioluminescence optical imaging (OI) are sensitive enough to detect molecular processes, but what they gain in sensitivity they lack in resolution [3]. Anatomical and molecular imaging modalities can be used in combination, such as in PET/CT, and SPECT/CT, where the CT scan provides anatomical information that is correlated or registered with the molecular information from the PET or SPECT scan.

A new molecular imaging modality, called Nanodiamond Imaging, is proposed that overcomes many of the limitations of the preclinical imaging techniques described above. Nanodiamond Imaging combines the high sensitivity of optical detection with the spatial resolving power of magnetic gradient-based imaging like MRI. Like the other molecular imaging modalities, Nanodiamond Imaging relies on the use of a tracer, or a material introduced into the organism and directly imaged, that can be attached to various biologically-relevant molecules. We use nanodiamonds containing a unique magneto-optical defect called the nitrogen-vacancy (NV) color center as a tracer, which can be quantitatively imaged to reveal the three-dimensional distribution of biologically relevant information. Applications such as monitoring gene expression patterns, diagnosis and longitudinal tracking of disease, stem cell tracking, and tumor detection are enabled by such tracer-based (molecular) imaging technologies [1].

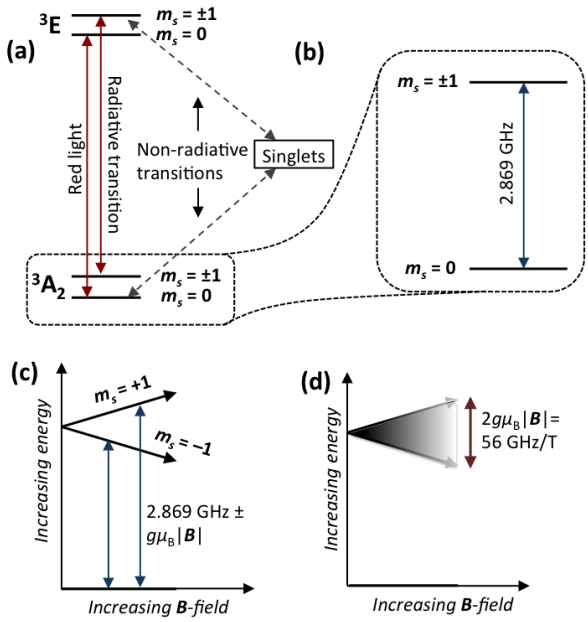

Figure 1. Level structure of NV. (a) Ground (^{3}A$_2$) and excited (^{3}E) electronic states shown with radiative transitions between like spin sublevels. Spin sublevels $m_s = \pm1$ of ^{3}E also decay non-radiatively to intermediate singlet states, enabling spin sublevel detection based on fluorescence intensity. The singlets decay preferentially to the $m_s = 0$ sublevel of the ground state, pumping the NV spin into that sublevel. (b) In the absence of a magnetic field, there is a microwave transition between $m_s = 0$ and $m_s = \pm1$ at 2.869 GHz. (c) A magnetic field along the NV spin axis splits the $m_s = +1$ and $m_s = -1$ transition lines. (d) An ensemble of NVs in a nanodiamond powder will show a transition that broadens with applied magnetic field, as the splitting for any one will be proportional to the projection of $\boldsymbol{B}$ along the NV spin axis.

A. Nitrogen-Vacancy Centers

Nitrogen-vacancy centers [4], [5] are bright optical emitters that can be excited in the red (600-630 nm) and fluoresce in the near-infrared (650-800 nm), at wavelengths that most readily penetrate tissue [6]. In the absence of a magnetic field, the ground state has a splitting of 2.869 GHz between the $m_s = 0$ and the $m_s = \pm1$ spin sublevels (see

*Research supported by the DARPA-QuEST program, the NSF Center for Scalable and Integrated NanoManufacturing (SINAM), and a Fannie and John Hertz Foundation P. Michael Farmwald Fellowship.

A. N. Hegyi (corresponding author; phone: 510-643-5801; e-mail: hegyi@eecs.berkeley.edu) and E. Y. Yablonovitch (e-mail: eliy@eecs.berkeley.edu) are with the Electrical Engineering Department, University of California, Berkeley, Berkeley, CA 94720 USA.

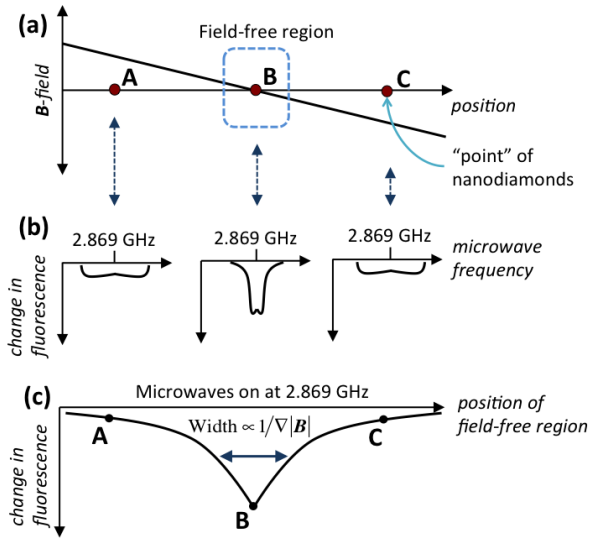

Figure 2. (a) A hypothetical one-dimensional magnetic field containing a field-free region. This field could exist on the line between two identical magnets with north poles facing each other. (b) Optically-detected magnetic resonance, as a function of microwave frequency, for points of nanodiamonds at locations **A**, **B**, and **C** in (a). The nanodiamonds at **B**, within the field-free region, show the strongest signal at the 2.869 GHz center frequency. (c) At 2.869 GHz, the microwave-induced change in fluorescence is dependent on the position of the nanodiamonds in the ***B***-field, relative to the field-free region.

Fig. 1). Introducing a magnetic field along the NV axis splits the $m_s = +1$ and $m_s = -1$ sublevels such that transitions from $m_s = 0$ occur at two different frequencies, 2.869 GHz ± 28 GHz/T. The NV has a long spin-relaxation time (T_1) of 1.2 ms [7] and a long spin coherence time (T_2) of greater than 1 us in nanodiamond [8].

As indicated in Fig. 1, the NV spin is pumped into the $m_s = 0$ sublevel upon optical excitation. The spin sublevel, whether $m_s = 0$ or $m_s = \pm 1$, can be detected via a spin-dependent fluorescence intensity: $m_s = \pm 1$ fluoresces more dimly than $m_s = 0$ because it can decay non-radiatively through the intermediate singlet states, whereas $m_s = 0$ decays primarily radiatively. However, even after the NV spins are pumped into the brighter $m_s = 0$ sublevel, exciting the microwave transition will mix the NV spin sublevels, leading to decreased fluorescence. Thus, microwave-induced spin transitions can be detected by a decrease in fluorescence intensity.

B. Nanodiamond

Several advantages of Nanodiamond Imaging come from the NV's nanodiamond host. Nanodiamonds are easily fabricated via a variety of methods, including high-pressure-high-temperature (HPHT) synthesis and detonation synthesis [9]. Typically NVs are created within the diamond via a high-energy implantation and annealing process. However, detonation nanodiamonds (DNDs) may be of greatest interest, as it is possible to create NV concentrations up to 1%, in a scalable way, by sintering of DND powder [10]. Nanodiamonds are easily functionalized to attach to a variety of biomolecules, for example by carboxylation [11]. Their

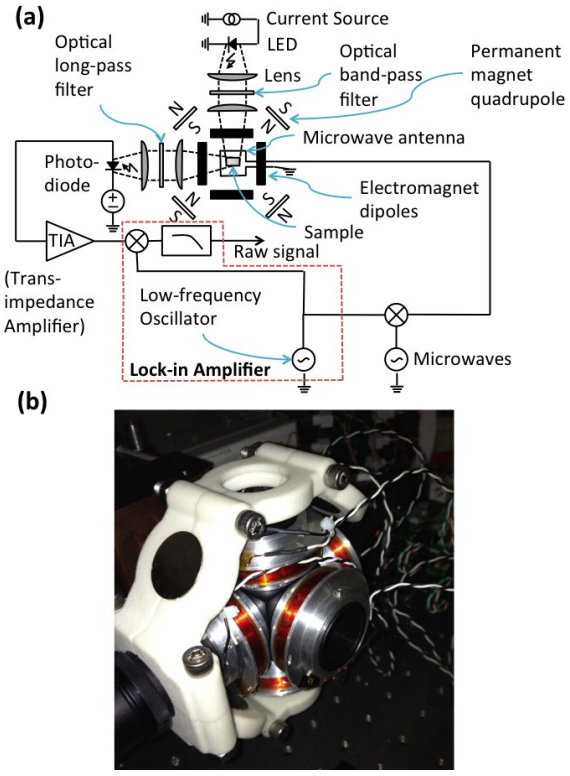

Figure 3. (a) Imaging system schematic. (b) Photograph of the magnetics subsystem and the central imaging chamber.

non-toxicity and immune system tolerance has been demonstrated in mice [12].

In this paper, we explain the fundamentals of how the new imaging modality works, and we demonstrate the first prototype system by imaging an artificial target, or a phantom, in tissue. We show how we will approach sub-100-µm resolutions and sensitivities better than 10 nM·mm^3·Hz$^{-1/2}$ concentration of carbon atoms.

II. Overview of Imaging System

The purpose of the imaging system is to detect the spatially-resolved concentration of nanodiamond tracer within an organism, or, from an optical point of view, within a highly scattering medium. The imaging system collects spatially-resolved, optically-detected magnetic resonance (ODMR) information from the sample, using a combination of magnetic, optical, electronic, and microwave subsystems.

An overview of how the ODMR signal is formed is shown in Fig. 2, and a schematic and picture of the imaging system is shown in Fig. 3. The sample is continuously irradiated with red light and microwaves at 2.869 GHz. A static magnetic field is present that has a field-free region—either a field-free point for creating three-dimensional images and two-dimensional slices, or a field-free line for creating two-dimensional projections. This field-free region can be rastered across the sample with additional magnetic fields. In Fig. 3, a field-free line is generated with a permanent-magnet quadrupole arrangement, and it is scanned across the sample with electromagnets. Within the

field-free region, the microwaves mix the NV spin sublevels, leading to dips in fluorescence. Because the dips in fluorescence can be a small (~0.1%) fraction of the total fluorescence, the microwaves are modulated enabling the corresponding changes in fluorescence to be detected synchronously with a lock-in amplifier. In the prototype system, the optical excitation is generated by a band-pass–filtered red LED, fed by a low-noise current source to minimize intensity fluctuations. Fluorescence is collected and condensed onto a photodiode, and the resulting photocurrent is sent to a transimpedance amplifier before being input to the lock-in amplifier. Note that the photodetector requires only a single element or pixel, and that spatial information about the nanodiamond concentration can be obtained solely from variations in fluorescence as the position of the field-free region is scanned.

III. Image with Current System

Two images as generated from the prototype system are shown in Fig. 4. Both are two-dimensional projection images made using a field-free line. The first image, in Fig. 4(a), is an image of a phantom (shown in Fig. 4(b)) that says "UC", which is made out of 6 pieces of 1 mm x 2 mm double-sticky tape with 2.5 µg of HPHT nanodiamond containing 6 ppm NVs on each piece of tape. This particular image was acquired outside of tissue. The imaging system was more sensitive to the right side of the phantom, which was closer to the photodiode. To correct for this non-uniform sensitivity, two images were recorded and registered on top of each other, with the phantom rotated 180° between images. The acquisition time was 1600 s for each 40 by 40 pixel image.

In the second image, Fig. 4(c), the phantom is a "C", 6 mm on a side, made out of 7 squares of 2 mm x 2 mm double-sticky tape, each coated with 5 µg of the same nanodiamond. The "C" is placed 8 mm beneath the surface of a 10 mm x 10 mm x 18 mm piece of chicken breast, as in Fig. 4(d). Chicken breast is a highly scattering tissue that homogenizes the sensitivity of the imaging system, thus making it nearly shift-invariant (i.e., the imaging system's point-spread function is independent of the location of a test point of nanodiamonds within the projection plane). The image as shown is deconvolved using a non-negative least-squares fit (with Tikhonov or minimum-norm regularization) to a point-spread function.

The point-spread function used in the deconvolution was derived by fitting a simplified, physically constrained functional form to measured data. The non-zero background in the raw image (Fig. 4(a)) comes from the wide tails of the point-spread function, which scales approximately as $1/r$, where r is the distance from the field-free region to the point of nanodiamonds. To see why the point-spread function has this scaling, we refer back to Fig. 1(d) and Fig. 2(b), where we see that the width (along the frequency axis) of the microwave transition, for an ensemble of nanodiamonds pointing in all directions relative to a magnetic field, increases linearly with the field strength. The amplitude of the ODMR at 2.869 GHz scales inversely with the width of

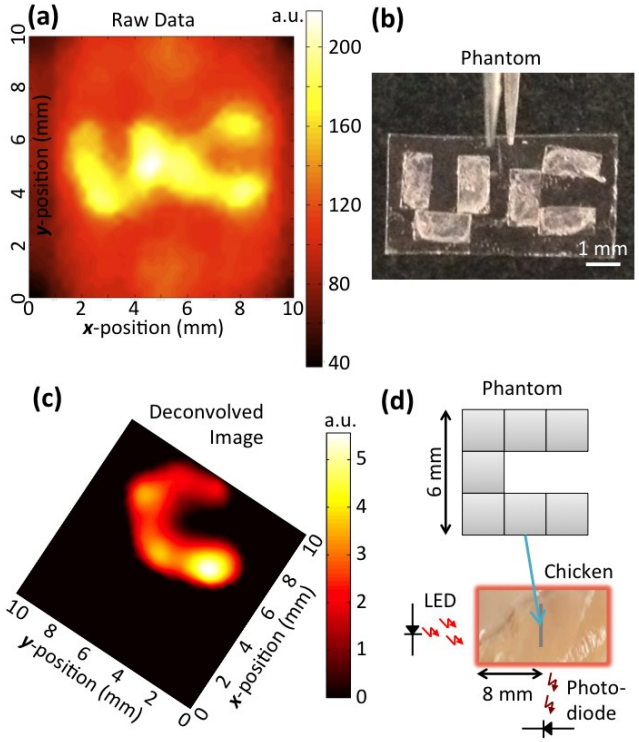

Figure 4. (a) Raw image data of phantom shown in (b), imaged outside of tissue. (b) Photograph of phantom made from double-sticky tape with a 1.25 µg/mm^2 areal density of nanodiamonds. (c) Image of phantom within chicken breast shown in (d), after deconvolution. Note the perfect background removal, in comparison to a raw image like (a). (d) Phantom made out of double-sticky tape with a 1.25 µg/mm^2 areal density of nanodiamonds, buried under 8 mm of chicken breast.

the microwave transition, hence the point-spread function decays inversely with the distance from the field-free region. Although it may appear that this point-spread function diverges at $r = 0$, the maximum signal is limited by strain within the nanodiamonds that broadens the 2.869 GHz transition.

A more accurate calculation of the point-spread function would take into account the spin Hamiltonian of the NVs in the magnetic field, the distribution of strain within the nanodiamonds, and the spatially varying optical and microwave excitation and fluorescence detection patterns.

IV. Performance

It is possible to quantify the performance of the current imaging system. Sensitivity and resolution were analyzed by placing a 0.3 mm x 0.3 mm piece of double-sticky tape in the imaging system, coated with 100 ng of nanodiamond. The observed peak signal (field-free line centered on the nanodiamond point) entering the lock-in was 50 µV, with approximately a 1 W/cm^2 illumination. The noise, primarily shot-noise from the non-modulated component of the photocurrent, was 2 µV·Hz$^{-1/2}$. Therefore, the sensitivity of this system is 4 ng·Hz$^{-1/2}$. Expressed in terms of concentration of carbon atoms, referenced to a (1 mm)^3 voxel, the sensitivity is 300 µM·Hz$^{-1/2}$. The half-width at half-max of the point-spread function, equivalent to the

system resolution, was approximately 500 μm, with a gradient of 1 T/m.

V. Discussion

We expect significant performance increases from foreseen improvements to the imaging system. First, we are using nanodiamonds with approximately 6 ppm NV, whereas it may be possible to create detonation nanodiamonds with up to 10,000 ppm NV via a sintering process [10]. Currently the measurement is carried out in a CW manner, although pulsing the measurement will provide a great benefit. The limiting factor to the signal strength is the intensity of the optical excitation, which must be controlled to prevent undue thermal load on the organism being imaged. However, the signal-to-noise ratio (SNR) increases with the 3/2 power of the optical intensity, because not only is more light collected (contributing the standard 1/2 power of optical intensity scaling of the SNR in shot-noise-limited systems), but the relative spin population, which determines the signal modulation depth, increases linearly with the optical intensity. Thus, it is advantageous to go to a pulsed scheme with a duty factor D ($0 < D < 1$), such that the signal collected in a given time and with a given amount of absorbed optical energy scales as D^{-1}.

More advanced coherent microwave pulsing schemes can be used if enough instantaneous microwave power is available to make the microwave Rabi nutation frequency surpass the decoherence rate of the NV spins. For example, the spins can first be optically pumped, and then they can be inverted periodically with a series of inversion (π) pulses while observing the resulting modulation of fluorescence. A coherent modulation scheme that inverts the spin population can produce up to twice the signal as an incoherent scheme, which can at best equalize the spin population between lower and upper levels. Furthermore, such a scheme would allow rastering much faster than the spin relaxation time T_1 because the spins would not have to relax to changes in the position of the field-free region.

Together these improvements should drive sensitivities to 10 $nM \cdot mm^3 \cdot Hz^{-1/2}$ or below. The reason sensitivity is expressed in this way is to decouple the sensitivity (in concentration units) from the voxel size and the measurement time, which unfortunately is not always done when comparing imaging techniques. To put the sensitivity in perspective, it is helpful to examine the following example. Assume we would like to image a 4 cm x 2 cm x 2 cm volume with 1 mm^3 resolution by acquiring a series of two-dimensional projections around the sample, to be combined using a projection reconstruction algorithm, as in a CT scan. We would like to image the volume in one minute, and we must collect 16,000 samples, so we have 3.75 ms per voxel. Since projection imaging is a multiplexed technique, each voxel will actually be sensed for 20x that time (field of view of 2 cm divided by voxel dimension of 1 mm), so sensitivity in each voxel will be better than 40 nM. If our sample is injected with 1 μmol or 12 μg of nanodiamonds and the nanodiamonds fill 10% of the voxels, those voxels will be imaged with an SNR approaching 15,000.

VI. Conclusion

Nanodiamond Imaging is a novel molecular imaging modality that can approach sub-100-μm resolutions with a 5 T/m static magnetic gradient field, and sensitivities approaching the $nM \cdot Hz^{-1/2}$ range for 1 mm^3 voxels. It can form two-dimensional projection images and three-dimensional renderings. Compared to other molecular imaging modalities such as PET and SPECT, there is no risk of ionizing radiation complicating the results of the imaging study, and the stable nature of the diamond particles allows much longer longitudinal studies than do radiotracers. The main drawback of the technique is depth penetration into tissue is limited to 2 to 3 cm, similar to fluorescence and bioluminescence imaging. However, unlike those imaging techniques, there is no loss of resolution with depth: the resolution is determined by the magnetic field gradient, which is unaffected by the presence of tissue.

Acknowledgment

A.H. thanks Patrick Goodwill, Steven Conolly, Michael Lustig, and Dennis Hegyi for discussion. Nanodiamonds were provided by Huan-Cheng Chang of the Institute for Atomic and Molecular Sciences, Academia Sinica, Taiwan.

References

[1] R. A. de Kemp, F. H. Epstein, C. Catana, B. M. W. Tsui, and E. L. Ritman, "Small-animal molecular imaging methods.," *Journal of nuclear medicine : official publication, Society of Nuclear Medicine*, vol. 51 Suppl 1, no. 1, p. 18S-32S, May 2010.

[2] M. A. Hahn, A. K. Singh, P. Sharma, S. C. Brown, and B. M. Moudgil, "Nanoparticles as contrast agents for in-vivo bioimaging: current status and future perspectives.," *Analytical and bioanalytical chemistry*, vol. 399, no. 1, pp. 3-27, Jan. 2011.

[3] S. R. Meikle, P. Kench, M. Kassiou, and R. B. Banati, "Small animal SPECT and its place in the matrix of molecular imaging technologies.," *Physics in medicine and biology*, vol. 50, no. 22, pp. R45-61, Nov. 2005.

[4] I. Aharonovich, A. D. Greentree, and S. Prawer, "Diamond photonics," *Nature Photonics*, vol. 5, no. 7, pp. 397-405, Jun. 2011.

[5] D. D. Awschalom, R. Epstein, and R. Hanson, "The diamond age of spintronics.," *Scientific American*, vol. 297, no. 4, pp. 84-91, Oct. 2007.

[6] V. Tuchin, Tissue Optics: Light Scattering Methods and Instruments for Medical Diagnosis, 1st ed. SPIE Publications, 2000, p. 5.

[7] D. Redman, S. Brown, R. Sands, and S. Rand, "Spin dynamics and electronic states of N-V centers in diamond by EPR and four-wave-mixing spectroscopy," *Physical Review Letters*, vol. 67, no. 24, pp. 3420-3423, Dec. 1991.

[8] J. Tisler et al., "Fluorescence and Spin Properties of Defects in Single Digit Nanodiamonds.," *ACS nano*, vol. 3, no. 7, pp. 1959-1965, Jul. 2009.

[9] A. Schrand, S. A. C. Hens, and O. Shenderova, "Nanodiamond Particles: Properties and Perspectives for Bioapplications," *Critical Reviews in Solid State and Materials Sciences*, vol. 34, no. 1, pp. 18-74, Jan. 2009.

[10] P. G. Baranov et al., "Enormously high concentrations of fluorescent nitrogen-vacancy centers fabricated by sintering of detonation nanodiamonds.," *Small (Weinheim an der Bergstrasse, Germany)*, vol. 7, no. 11, pp. 1533-7, Jun. 2011.

[11] J.-I. Chao et al., "Nanometer-sized diamond particle as a probe for biolabeling.," *Biophysical journal*, vol. 93, no. 6, pp. 2199-208, Sep. 2007.

[12] E. K. Chow et al., "Nanodiamond therapeutic delivery agents mediate enhanced chemoresistant tumor treatment.," *Science translational medicine*, vol. 3, no. 73, p. 73ra21, Mar. 2011.